Design of nanofilters for optical nanocircuits

Andrea Alù, Michael E. Young, and Nader Engheta*

University of Pennsylvania, Department of Electrical and Systems Engineering, Philadelphia, Pennsylvania 19104, USA

(Received 2 October 2007; revised manuscript received 16 December 2007; published 9 April 2008)

We theoretically and numerically study the design of optical "lumped" nanofiltering devices in the framework of our recently proposed paradigm for optical nanocircuits. In particular, we present a design of basic filtering elements, such as low-pass, pass-band, stop-band, and high-pass lumped nanofilters, for use in optical nanocircuits together with more complex designs, such as multizero or multipole nanofilters, to work at THz, infrared, and optical frequencies. Following the nanocircuit theory, we show how it is possible to design such complex frequency responses by applying simple rules, similar to those in rf circuit design, and we compare the frequency response of these optical nanofilters with classic filters in rf circuits. These findings introduce a theoretical foundation for the fabrication of nanofilters in optical lumped nanocircuit devices.

I. INTRODUCTION

The importance of transplanting classical circuit concepts into optical frequencies is based on the possibility of squeezing circuit functionalities (e.g., filtering, waveguiding, multiplexing, etc.) in subwavelength regions of space and of correspondingly increasing the operating frequency with several orders of magnitude. Moreover, current interest in combining optical guiding devices, as optical interconnects, with micro- and nanoelectronic circuits is high (see, e.g., Ref. [1]), since it is still not possible to perform all classic circuit operations in the optical domain. Introducing new paradigms and feasible methods to bring more circuit functionalities into the optical domain would represent an important advance in nanoelectronics technology.

In a recent Letter,[2] we have introduced and discussed the fundamental concepts for developing a novel paradigm for optical nanocircuits, with the aim to extend classic circuit concepts, commonly available at rf and lower frequencies, to higher frequencies, and in particular to the optical domain. Specifically, we have discussed in Ref. [2] and in following papers[3–10] how a proper combination of plasmonic and nonplasmonic nanoparticles may constitute a complex nanocircuit at infrared and optical frequencies, for which the conventional lumped circuit elements are not commonly available. After introducing the nanocircuit concepts for isolated nanocircuit elements,[2] and after having applied them to model infinite stacks of nanoelements to design nanotransmission lines and nanomaterials,[4–6] we have analyzed in detail how the connections and interactions among the individual nanoelements may be modeled and designed in a complex optical *nanocircuit board* with functionalities corresponding to those of a classic microwave circuit. In Refs. [7–9] we have indeed analyzed basic coupling issues among individual nanocircuit elements and we have proposed the use of ε-near-zero (ENZ) and ε-very large (EVL) materials, with ε being the local material permittivity, in order to operate as "insulators" and "connectors," respectively, for proper interconnections among the different elements of a nanocircuit systems. In Ref. [10] we have also proposed a specific geometry to model a "shorting wire" at optical frequencies, in order to connect relatively "distant" sections of a nanocircuit board. A recent review of some of these concepts and potential applications for optical nanocircuits has been presented in Ref. [3].

The interest in interpreting the light interaction with plasmonic materials in terms of circuit models has been reported in earlier literature (see, e.g., Refs. [11–15]). However, the novelty of our approach[2] consists in the ability to tailor and design nanoparticles to act as "lumped" circuit elements (e.g., nanoinductors, nanocapacitors, and nanoresistors) with given lumped impedances at optical frequencies. From this concept, one will then be able to *quantitatively* design and synthesize more complex nanocircuits and nanosystems at optical frequencies, combining collections of nanoparticles acting as "lumped" nanocircuit elements as in a conventional circuit board. As we have discussed in Ref. [2], in fact, a complete equivalence between rf circuits and optical nanocircuits relies on the analogy between the local conduction current density ($\mathbf{J}_c = \sigma\mathbf{E}$) and the local displacement current density ($\mathbf{J}_d = -i\omega\varepsilon\mathbf{E}$), with σ and ε being the local material conductivity and permittivity, respectively, and $\mathbf{E}$ the local electric field. The proportionality of $\mathbf{J}_d$ with frequency, added to the usual frequency dispersion of the material permittivity ε, which generally follows the Drude-Lorenz dispersion models,[16,17] implies that at higher frequencies the role of conduction current in optical nanocircuits is overtaken by the role of $\mathbf{J}_d$.[2] This explains why the role of conductivity σ in low-frequency circuits is "replaced" by the local permittivity ε in optical nanocircuits. As we mentioned in Ref. [2], it follows that plasmonic (negative ε) and dielectric (positive ε) nanoparticles may constitute, respectively, lumped nanoinductors and nanocapacitors, whereas ENZ or EVL materials in this paradigm correspond, respectively, to "poor conductors," or nanoinsulators, and "good conductors," or nanoconnectors.[7] With these tools, it is possible to envision more complex interconnections among the different lumped nanocircuit elements, or even nanomodules, of a nanocircuit board, in order to realize complex frequency responses at infrared or optical frequencies.

Following this same analogy between classic circuit theory and these optical nanocircuits, in the following we go one step further to present a complete analysis and some designs for nanoscale filtering modules at optical frequencies. In this scenario, we apply the familiar concepts of cir-

cuit and filter theories, in order to design first- and second-order nanofilters (in Sec. II) and higher-order nanofilters (in Sec. III) with complex frequency responses by combining and juxtaposing up to four reactive nanoelements. Our results seek to pave the way for the future design of functional lumped optical nanocircuits at frequencies where the classic rf lumped circuit elements are no longer available.

II. BASIC FILTERING ELEMENTS: FIRST- AND SECOND-ORDER OPTICAL NANOFILTER DESIGN

The fundamentals of filter design in low-frequency circuits are based on the frequency responses of lumped capacitors and inductors[18] and their combinations. For instance, a standard low-pass or high-pass filter is based on the voltage extracted from a resistor-capacitor (*RC*) pair or a resistor-inductor (*RL*) pair, respectively. An inductor-capacitor (*LC*) pair, due to its inherent resonant properties, constitutes the fundamental pass-band or stop-band filter. In this section we consider these basic elements as the starting point for our lumped optical nanofilter design. In particular, in the following we will consider nanocircuits embedded in a parallel-plate waveguide, which guides the input optical excitation. Following the theoretical results reported in Ref. 2, all the nanocircuit elements will be subwavelength in size at the frequency of interest, in order to allow them to function as lumped elements. For the sake of simplicity, the structures analyzed here are two dimensional (2D), and the cross sections of all of our nanostructures (i.e., nanorods) studied here are small compared with the operating wavelengths. Extension to a fully 3D geometry would not change the main concepts presented here. The numerical results are fully dynamic, extracted from full-wave simulations by commercially available finite-integration time-domain software,[19] in some examples also compared to finite-element software,[20] and consider realistic dispersion and reasonable losses for the involved materials. In all of the examples, the results are compared with what is expected from an analogous design in a low-frequency rf circuit, considering the quantitative values of the involved nanocircuit elements as predicted by nanocircuit theory,[2] and in each case a sketch of the related circuit model is shown.

As already mentioned, the functionalities of the lumped nanofilters considered here have been evaluated inside a parallel-plate waveguide, which may correspond at optical frequencies to a metal-insulator-metal waveguide (see, e.g., Refs. 4 and 21). In different setups, the waveguide walls may be substituted by the boundaries of a photonic crystal or by an integrated waveguide, with the similar purpose of suppressing unwanted radiation from the loads. Analogous responses may also be expected when the same nanocircuit elements are employed in different setups—e.g., when printed on a substrate[9] or when utilized as "loads" in optical nanoantennas—as we have recently suggested in Refs. 22 and 23. Such geometries, which may be closer to a practical realization at optical frequencies, go beyond the interest of the present work, in which we aim to fully characterize the nanofiltering response of proper combinations of nanocircuit elements, disengaged from the possible dispersion of plas-

monic waveguides, substrates, or nanoantennas. Since the goal of the present work is to determine the filtering transfer functions of collections of nanoelements, therefore, here we have assumed that the host waveguide is made of perfectly electric conducting (PEC) walls (i.e., wall with infinite conductivity) and thus a transverse electromagnetic (TEM) mode is launched at the input of this waveguide. The frequency response of this "empty" waveguide may be consequently assumed to be uniform and flat. In a realistic scenario, the metallic walls of the waveguide are dispersive and thus the waveguide itself may exhibit certain well-known (relatively weak) dispersion, as analyzed in Ref. 4, which will "modulate" the filtering function of the nanofilters. This additional dispersion may of course be fully taken into account in any realistic design of such nanofilters. Furthermore, as can be implied from our work in Ref. 4, the major portion of electromagnetic fields in the metal-insulator-metal waveguide is located in the dielectric region of this waveguide where the nanofilter elements is located, and thus will interact fully with these nanoelements.

A. Low-pass optical nanofilter: Parallel *RC* combination

As a first example, Fig. 1 reports the design of a low-pass nanofilter. The geometry is sketched in the inset and is represented inside the cross section of a parallel-plate waveguide (with the impinging electric field oriented from bottom to top of the figure) in air (permittivity ε_0). The low-pass nanofilter is formed as an "*RC* parallel combination," as the circuit sketch reports in the inset of the figure, where the parallel resistance is provided by the intrinsic impedance of the waveguide η. The "nanocapacitor" C is formed by a dielectric nanorod of permittivity $\varepsilon_C = 16\varepsilon_0$ (close to silicon-based materials at infrared-optical frequencies) with base $d = 20$ nm and height $h = 10$ nm. The geometrical and electromagnetic parameters have been chosen as possible design values, but the concepts outlined here are in principle scalable to different frequencies or different material parameters.

The parallel-plate waveguide has a total height $h_{wg} = 100$ nm and it is closed on top and bottom by perfect electric conductors (i.e., with infinite conductivity), which may well represent some impenetrable metal with sufficiently negative permittivity in the frequency regime of interest. The "nanocapacitor" is connected to the protrusion attached to the bottom of the waveguide, which is made of a material with sufficiently large (positive or negative) permittivity (EVL), for which the corresponding impedance is low enough to act as a short circuit, consistent with our findings in Refs. 7 and 10 [we note here that the ENZ and EVL material parameters employed in this simulation may arguably be hard to find in nature at the frequency of interest, but "layered" ENZ and EVL metamaterials may be straightforwardly designed by stacking together plasmonic (e.g., noble metals) and nonplasmonic (e.g., dielectric) thin-layered materials with the proper orientation with respect to the electric field, as considered in Refs. 24 and 25]. The capacitance per unit length of the nanoparticle may be evaluated following Ref. 2, yielding $C = \varepsilon_C d/h = 0.283$ nF m^{-1}. The parallel "resistance" R of the nanofilter, as mentioned above, is provided
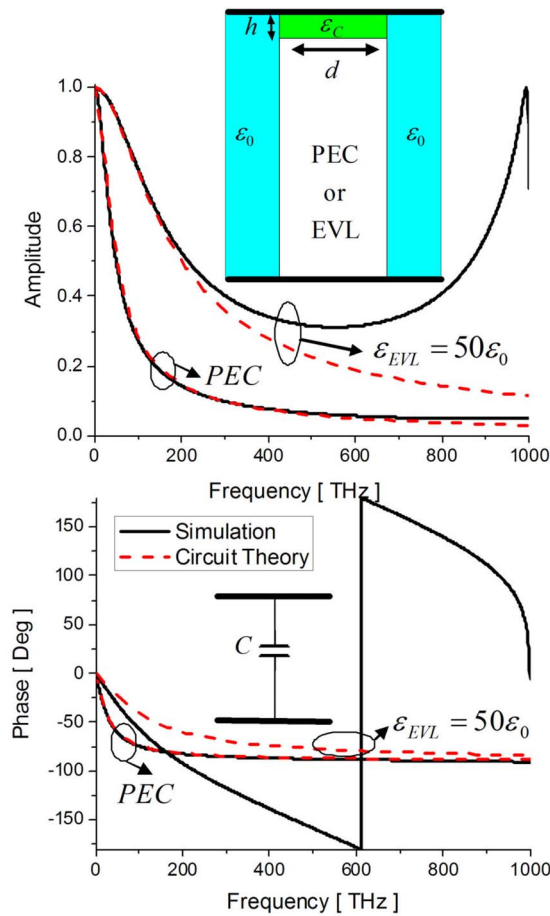
FIG. 1. (Color online) Transfer function (amplitude and phase) for the basic low-pass optical nanofilter made of a dielectric nanorod in a waveguide, as depicted in the inset. The black solid lines refer to full-wave simulations, whereas the red dashed lines correspond to circuit-theory calculations for the circuit model sketched in the inset.

by the characteristic impedance of the waveguide, which in this geometry is given by $\eta = \sqrt{\mu_0/\varepsilon_0}h_{wg} = 18.85\ \mu\Omega$ m, with μ_0 being the permeability of free space.

The extracted transfer function for this basic optical nanofilter is shown in Fig. 1, in amplitude and phase (black lines), and it is compared with the one obtained through the circuit theory for the same values of R and C. Simulations have been performed both for an ideal PEC step (i.e., a step with infinite conductivity) and for an EVL material with $\varepsilon_{EVL} = 50\varepsilon_0$. In the ideal PEC scenario, the agreement between the lines is quite good, despite the drastic abruption in the waveguide cross section and the dynamic nature of the problem, which does not consider any "nanoconnector" or "nanoinsulator" around the element. This is due to the small dimensions of the nanocircuit with respect to the wavelength of operation and to the absence of a resonant response, which ensures the "lumped" behavior of the nanocircuit over the frequency range of interest. A very minor discrepancy in the amplitude and phase of the extracted transfer function is seen at higher frequencies, when the nanocapacitor size becomes closer to the wavelength of operation. The amplitude of the
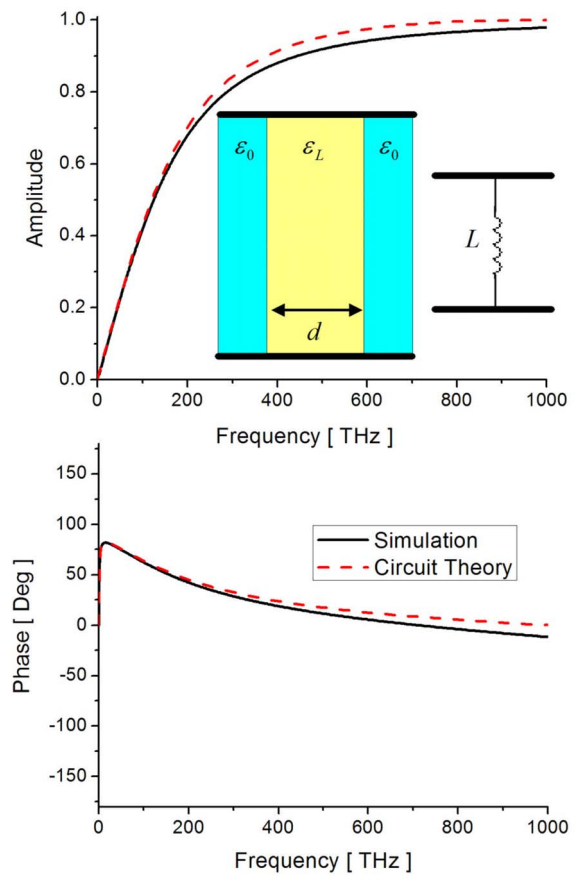

FIG. 2. (Color online) Transfer function (amplitude and phase) for the basic high-pass optical nanofilter formed by a plasmonic nanorod in a waveguide, as depicted in the inset. The black solid line refers to full-wave simulations, whereas the red dashed line corresponds to the circuit-theory calculations for the circuit model sketched in the inset.

nanofilter rapidly decays in frequency, and the phase passes from 0 to $-90°$, consistent with the functionality of an RC-parallel low-pass filter.

When a positive-permittivity protrusion is considered, like in the second set of curves with $\varepsilon_{EVL} = 50\varepsilon_0$, the full-wave simulations match the circuit theory in the low-frequency range. However, at higher frequencies the wavelength inside the EVL material may become comparable with the size of the nanocircuit element, and therefore the lumped circuit theory loses its applicability in this particular example. This explains the discrepancy between the full-wave simulation and rf circuit model curves at higher frequencies. The low-pass filter still retains its function for frequencies until about 500 THz in this example.

It should be noted that the waveguide step has been inserted in this geometry simply to increase the value of the small capacitance with respect to the characteristic impedance of the waveguide, in order to fine tune the low-transmittance frequency of the RC nanofilter in the visible range and to highlight the functionalities of this basic low-pass nanofilter. In other geometries, such as when loading a nanoantenna[22,23] or a different waveguide setup, such a pro-
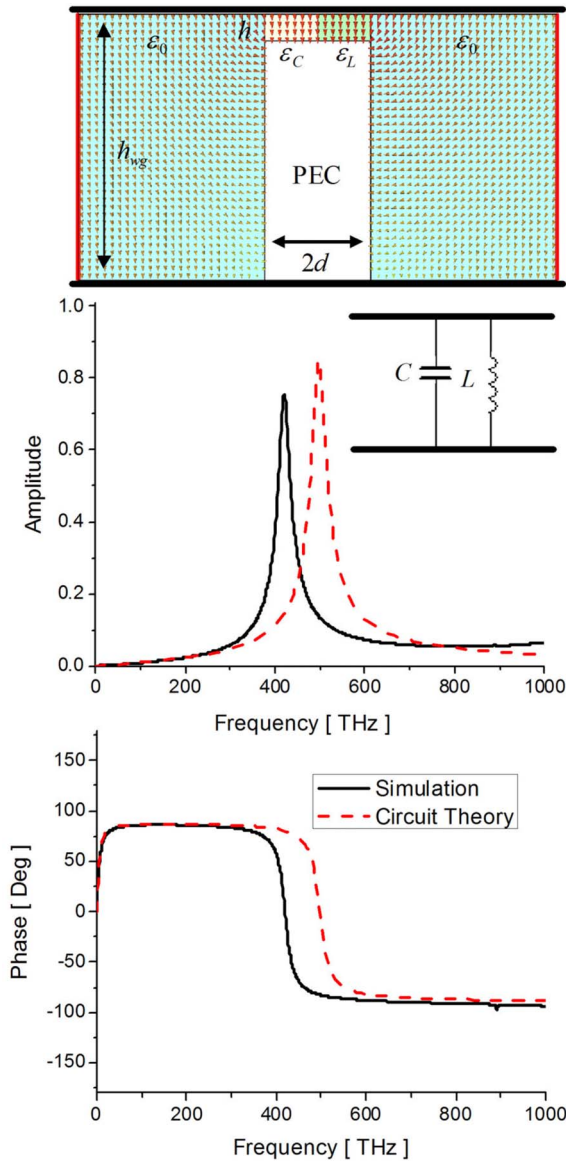
FIG. 3. (Color online) Transfer function (amplitude and phase) and electric field distribution at the resonance for an optical pass-band nanofilter formed by two nanorods juxtaposed in parallel in a waveguide, one made of silicon and the other made of silver.

trusion may not be required. Here the step geometry may provide an interesting additional tool to tailor the frequency response of the filter for the designer's needs. The choice of size and permittivity for the nanocapacitor in Fig. 1 is arbitrary, and variations in the geometry or properties of the involved nanoparticles, here as well as in the following examples, may be easily taken into account as a variation of the corresponding lumped impedance, as calculated in Ref. 2. This implies that the size, geometry, and properties of the nanoelements eventually determine the filtering response of the nanocircuit and their variation would tune this response as in a standard low-frequency rf circuit. In the design, these parameters provide several degrees of freedom for tailoring the frequency response of the nanofilter at will.
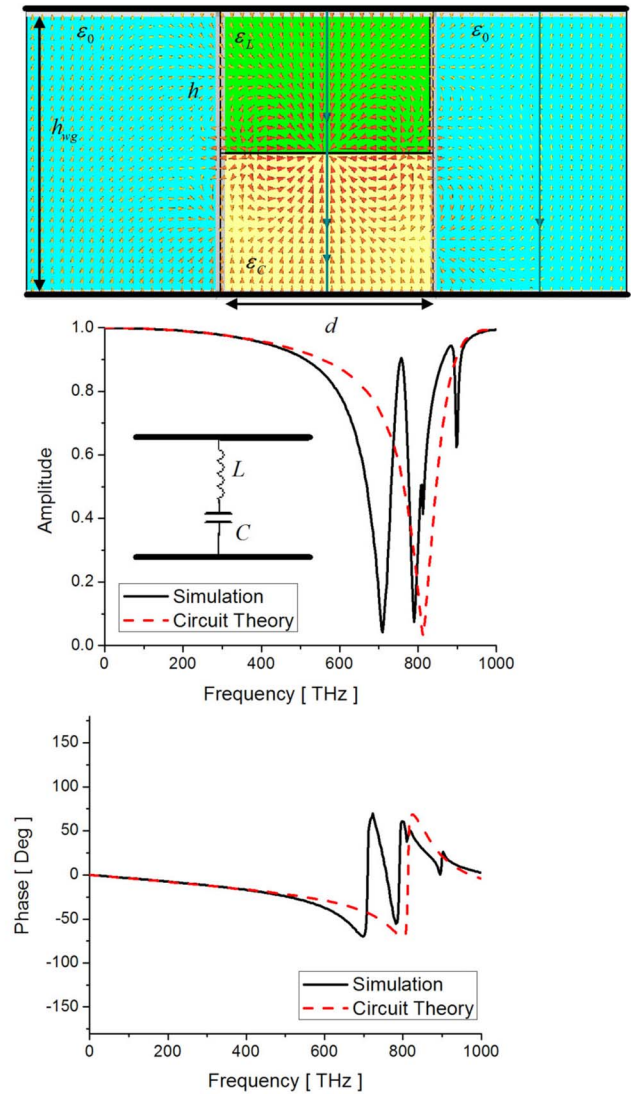

FIG. 4. (Color online) Electric field distribution at resonance and the transfer function for a stop-band nanofilter formed by two nanorods juxtaposed in series in a waveguide, one made of silicon dioxide and the other made of silver.

B. High-pass optical nanofilter: Parallel *RL* combination

A simple high-pass filter is depicted in Fig. 2. It is formed as an "*RL* parallel combination," where the "nanoinductor" *L*, as first suggested in Ref. 2, is a plasmonic nanorod with cross sectional dimensions $(h_{wg}=100 \text{ nm}) \times (d=20 \text{ nm})$. This nanorod has a permittivity following a Drude model: i.e.,

$$\varepsilon_L = \varepsilon_0 \left(1 - \frac{f_p^2}{f(f+i\gamma)} \right), \qquad (1)$$

with $f_p = 10^3$ THz and $\gamma = 1$ THz, which models reasonable dispersion and losses for a plasmonic material at infrared and optical frequencies. Also in this case the "resistance" *R* is provided by the characteristic impedance of the waveguide. Again, full-wave simulations and circuit predictions coincide
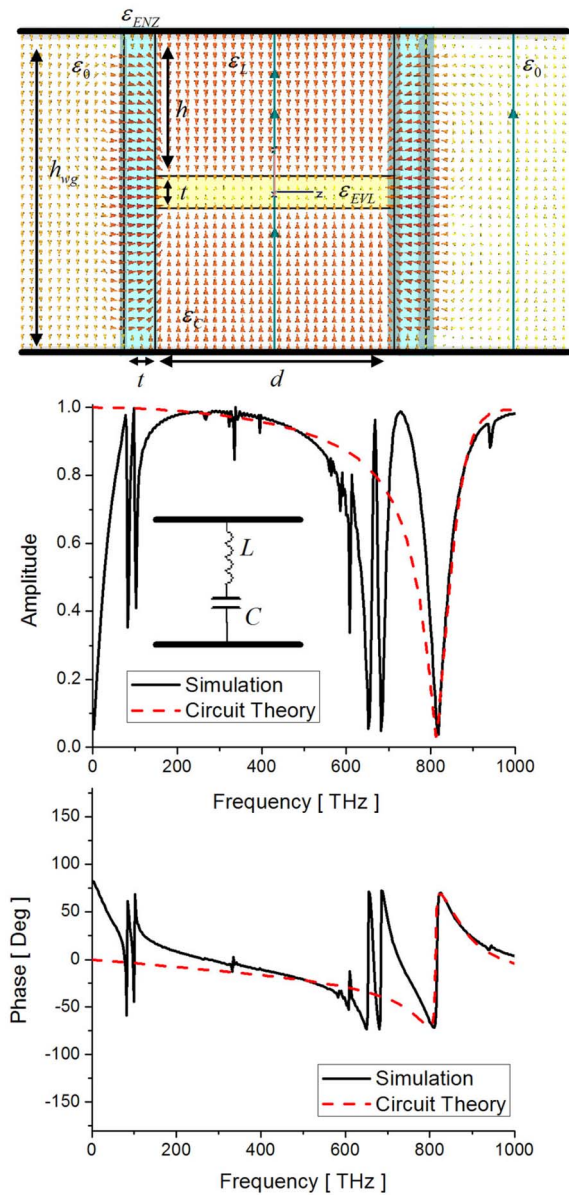
FIG. 5. (Color online) Similar to Fig. 4, except here ENZ nano-insulators and EVL nanoconnectors improve the nanocircuit functionality.

very well, and the high-pass functionality of this nanofilter is evident from the plots in Fig. 2.

It should be noted that in this example the nanoinductor has some intrinsic small losses included in it, due to the absorption of the plasmonic material. Moreover, the value of the associated equivalent inductance per unit length of this nanorod is inherently dispersive, generally changing with frequency following the formula $L = -\frac{h_{wg}}{\omega^2 \varepsilon_L(\omega) d}$.[2] These aspects are fully taken into account in the nanocircuit model. The presence of losses in the material explains why the phase of the transfer function goes abruptly to zero at very low frequencies. The smooth transition of the phase from $+90°$ to zero is typical of a high-pass RL filter. As an aside, we note that for frequencies sufficiently lower than f_p, but still

greater than γ, the value of ε_L becomes approximately $\varepsilon_L \simeq -\frac{\omega_p^2}{\omega^2}$, which results in an approximately constant effective inductance per unit length $L = \frac{h_{wg}}{\varepsilon_o \omega_p^2 d}$.

It should also be underlined here that at high frequencies the size of the nanoinductor may become comparable with the skin depth of the metal in this, as well as in some other following examples. Although the functionality of the nano-filter is evidently correct (Fig. 2), the minor deviation between full-wave simulations and circuit theory may be in part associated with the fact that the electric field may have a somewhat lower amplitude at the center of the nanoinductor, due to its skin depth. Being based on a quasistatic analysis which assumes uniform field distribution all over the par-ticle, the circuit theory does not take into account this effect, whereas the full-wave simulation does. This may explain the minor deviation between solid and dashed lines at high fre-quencies in this and some of the following examples.

C. Pass-band optical nanofilter: Parallel *RLC* resonance

Figure 3 reports the design of a "parallel *RLC*" optical nanofilter working as a pass-band device. The nanofilter was designed by juxtaposing two nanorods with cross-sectional dimensions $(d = 20 \text{ nm}) \times (h = 10 \text{ nm})$. The two nanoelements have, respectively, permittivity $\varepsilon_C = 14.15\varepsilon_0$, which corresponds to the permittivity of silicon at optical frequencies[26] and $\varepsilon_L = (5 - \frac{f_p^2}{f(f+i\gamma)})\varepsilon_0$, where $f_p = 2175$ THz and $\gamma = 4.35$ THz, which models silver at optical frequencies.[27] Once again, the two nanorods have been em-bedded in the waveguide by positioning them on top of a step made of an impenetrable material (i.e., material with infinite conductivity, the same that composes the parallel plates on top and bottom of the waveguide). The geometry in the figure shows the distribution of electric field in the wave-guide at the resonance frequency, which occurs at 420 THz.

Consistent with our analysis in Ref. 8, the two nanocircuit elements are in parallel due to the orientation of the imping-ing optical electric field (parallel to the common interface) and the optical potential drop from the top to the bottom of the two nanoelements is indeed the same. The equivalent circuit is shown in the inset of Fig. 3, and the corresponding
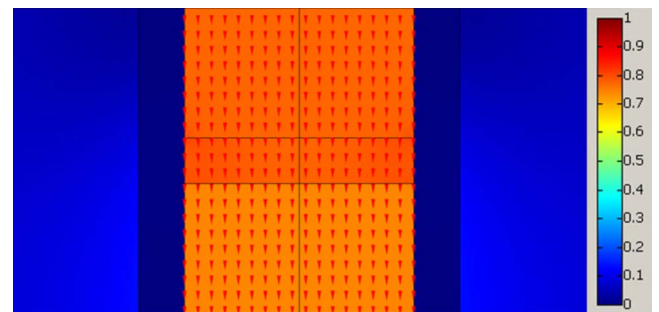

FIG. 6. (Color online) Electric displacement distribution at reso-nance for the stop-band nanofilter of Fig. 5, simulated using finite-element software (Ref. 20). The color scale refers to the displace-ment vector amplitude (snapshot in time, arbitrary units), whereas the arrows refer to its direction.
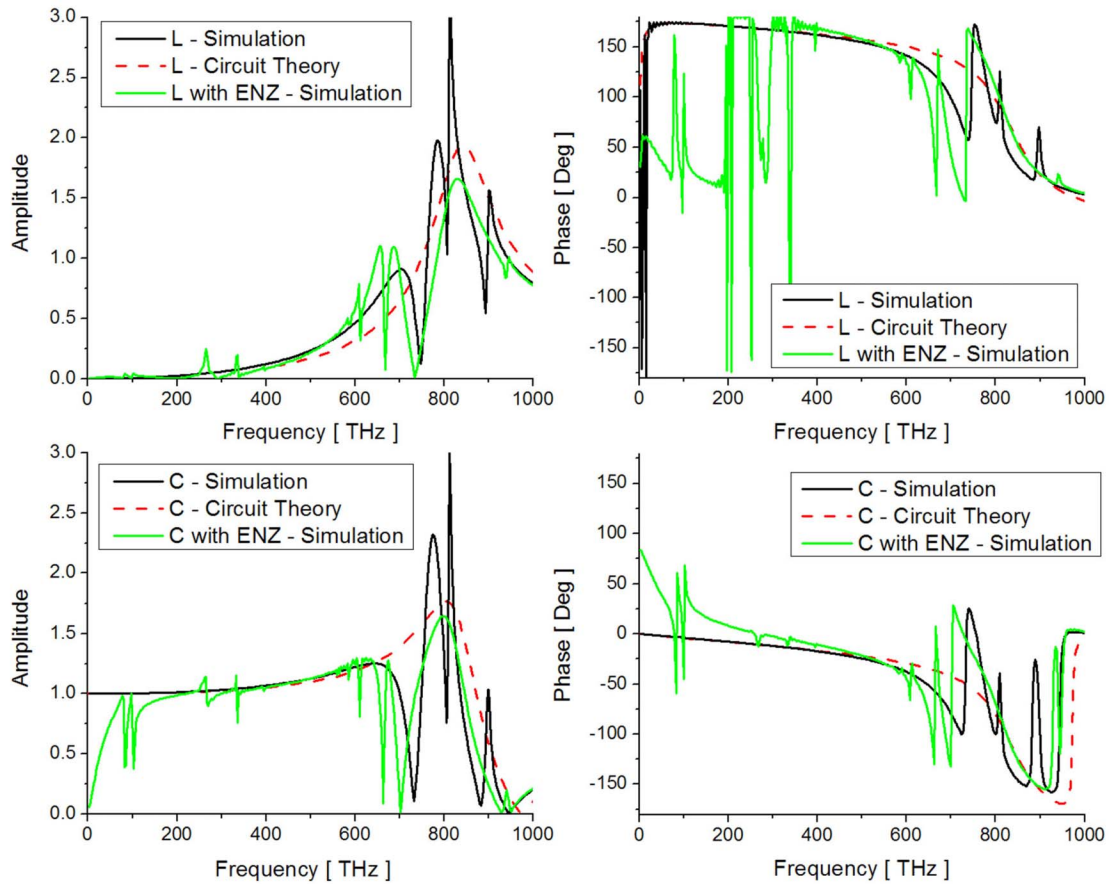
FIG. 7. (Color online) Extraction of the amplitude and phase of the normalized electric field (with respect to the incident field) across the individual *L* and *C* nanoelements in the scenarios of Fig. 4 (black solid line) and Fig. 6 (green light line), compared to the ideal circuit.

transfer function is compared with the simulated one in the plots. The simulated and theoretical results match reasonably well, in both amplitude and phase, despite a small shift in the resonance frequency, due to the evident mismatch between the waveguide cross section and the nanoparticle cross section at the resonance. Since the two nanorods have the same cross-sectional dimensions, from the circuit theory the resonance is expected to occur when the two material permittivities have the same magnitudes but opposite signs—i.e., around 500 THz. The actual resonance is shifted down, possibly due to the local fringing fields at the waveguide abruption that slightly increase the value of *C*. It is also evident how the presence of resonances in the nanocircuit slightly detunes the expected transfer function from the simulated one, when compared with the previous examples. Nevertheless, the agreement between the two lines is reasonably good, and with a proper optimization, or the use of nanoinsulators and nanoconnectors, this may be improved.

As in the low-pass nanofilter case, the choice of reducing the height *h* of the nanoelements with respect to the height of the waveguide h_{wg}, using a suitable PEC or EVL (not shown here) protrusion, is motivated by the possibility of increasing the value of *C* and simultaneously reducing the value of *L*, following the previous formulas. In this case, the *Q* factor of the "parallel-*RLC* resonance," given by the standard expression[18]

$$Q = R \sqrt{\frac{C}{L}}, \qquad (2)$$

increases, and therefore the pass band becomes narrow around the frequency of interest. As we discussed in the case of low-pass nanofilters shown in Fig. 1, the use of EVL materials for this step has its own constraint, and therefore this EVL step design should be done judiciously such that the frequency range of its applicability would include the desired pass-band center frequency.

If we considered $h = h_{wg}$, we would indeed get the advantage of no abruption in the waveguide section and therefore a better agreement between the circuit theory and full-wave simulations. However, in this case the bandwidth of operation of the filter would become larger.

As suggested in Ref. 7, the use of proper ENZ nanoinsulators on the "front" and "back" of the nanocircuit, in order to confine the undesired displacement current leakage out of the resonant pair in this case for which $h < h_{wg}$, might improve the agreement between circuit theory and simulations around the resonance frequency.

The material permittivities, dimensions of the nanorods' cross sections, and the height of the step represent degrees of freedom in the design to achieve the required frequency response for the pass-band filter, in terms of both central frequency and bandwidth of operation.
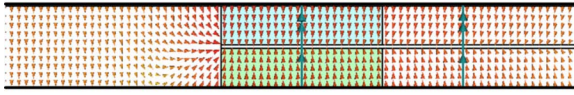
FIG. 8. (Color online) Electric field distribution at the resonance for a stop-band nanofilter made by a SiO_2 and a silver nanorod in the series combination. An EVL nanoconnector is used to extract the optical voltage drop across each of the two nanoelements and "carry" them to the output end of the waveguide.

D. Stop-band optical nanofilter: Series *LC* resonance

Up to now we have limited our analysis to parallel combinations of nanocircuit elements for realizing simple nanofiltering systems. We recall here that, as shown analytically in Ref. 8, two nanocircuit elements may be considered in parallel when the orientation of the impinging electric field is parallel to their common interface, as was the case in the previous scenarios. The series interconnection in this paradigm corresponds to the case in which the electric field is orthogonal to the common interface between the two nanoelements, and therefore the displacement current flows continuously from one element to the other ideally without current leakage in the surrounding circuit, as between two series elements in a standard rf circuit.

Due to the specific geometry being studied here, the parallel configuration allows better matching between the impinging wave phase fronts inside the waveguide and the nanocircuit. However, if we stack a resonant *LC* nanopair in series, rather than in parallel, as in Fig. 4, we may realize a stop-band nanofilter, consistent with the circuit model in the inset of Fig. 4. More generally, such series configurations may provide extra design tools for tailoring the frequency response of a complex nanocircuit. In this subsection, we analyze in detail the possibility of using a resonant series combination of nanoelements to design a stop-band nanofilter.

Figure 4 provides an example of such a resonant series configuration. A SiO_2 nanorod, with permittivity $\varepsilon_C = 2.16\varepsilon_0$,[28] has been stacked over a silver nanorod with the same cross-sectional dimensions: $h = h_{wg}/2 = 10$ nm and $d = 15$ nm. In this way, a series resonance may "short" the waveguide and create a stop band, expected at around 800 THz for this example. Due to the abruption of the waveguide and the strong value of the fringing fields around the interface between the two nanorods near the resonant frequency, the response of the nanofilter is slightly more complex than what the equivalent rf circuit theory would predict, but still the response in amplitude and phase approximately recalls the general trend predicted by the circuit theory (with additional resonances present due to the plasmonic resonance at the *interface* between the plasmonic and insulating materials or between the plasmonic and dielectric materials). This effect may introduce further flexibility and tunability of the frequency response of the nanofilter, due to the presence of additional localized plasmonic resonances. It is worth noting, however, that these additional stop bands shown in Fig. 4 occur at about 50 THz below and above the main stop band predicted by the circuit theory and therefore allow a rela-
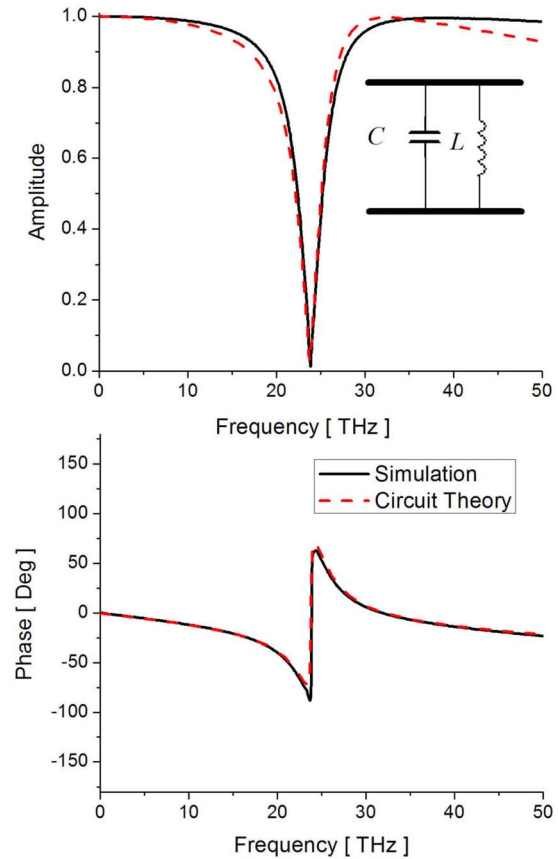

FIG. 9. (Color online) Frequency response of the parallel combination of a SiC and a dielectric nanorod at THz frequencies.

tively large frequency band of operation around the main stop band. This implies that if the desired operational band of a system is about 800 ± 25 THz, for the example shown in Fig. 4, the main stop band of the pair of nanorods will be the main one predicted by the circuit theory.

It is important to note that the field distribution at the resonance of the nanofilter, reported in Fig. 4, indeed resembles that of a resonant *LC* series: the electric field is oppositely oriented and very strong at the interface between the two nanocircuit elements, in order to provide a continuous displacement current flowing across the resonant pair with a zero voltage drop. This is consistent with our analytical findings in Ref. 8.

In order to better improve the agreement between the circuit theory and the full-wave simulations around the stop band, we have simulated in Figs. 5 and 6 the same geometry, but with added two tiny layers ($t = 3$ nm thick) of ENZ nanoinsulators on the front and the back of the nanocircuit pair and a layer of EVL connector between the resonant pair. This was done to limit the displacement current leakage at the resonance around the pair and to reduce the effect of plasmonic resonance at the interface between the two elements. The ENZ material was designed assuming a Drude model (1) with plasma frequency selected to be at the resonance frequency of the circuit, whereas the EVL material was assumed to have a permittivity $\varepsilon_{EVL} = 100\varepsilon_0$. (One may also use
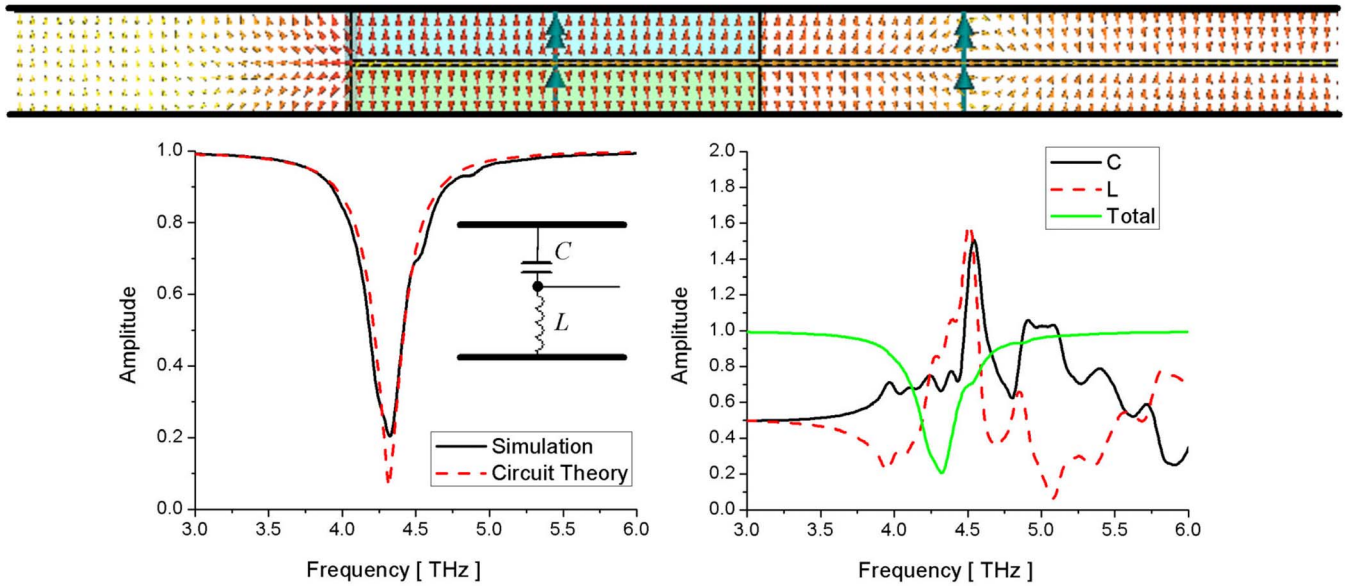
FIG. 10. (Color online) Electric field distribution at the stop-band frequency, transfer function of the nanofilter, and extraction of the normalized field across the terminals of each of two nanocircuit elements for an *LC* series combination at THz frequencies.

an EVL with negative permittivity, as we discuss and prove analytically for a different geometry in Ref. 10.)

It is clear in Fig. 5 how the agreement between black (solid) and red (dashed) lines around the stop band is better with these additions; however, the intrinsic Drude dispersion of the ENZ material at lower frequencies causes the ENZ to become an epsilon-negative (ENG) layer, which consequently affects the frequency response at lower frequencies, effectively adding to the resonant pair two nanoinductors in parallel that modify the overall response of the circuit at lower frequencies. Even if in this setup the use of ENZ and EVL materials is not crucial, in more complex nanocircuits their use turns out to be important in order to avoid unwanted coupling among nanocircuit elements.[7] We note here that the ENZ and EVL material parameters employed in this simulation may arguably be hard to find in nature at the frequency of interest, but "layered" ENZ and EVL metamaterials may be straightforwardly designed by stacking together plasmonic (e.g., noble metals) and nonplasmonic (e.g., dielectric) thin-layered materials with the proper orientation with respect to the electric field, as considered in Ref. 25. Our preliminary results and simulations in this sense confirm that it is possible to exploit this technique to fabricate artificial ENZ and EVL metamaterials with the proper frequency response for our nanocircuit applications.

The electric field and displacement distribution in Figs. 5 and 6, extracted at the resonance frequency of the circuit, show how the ENZ insulators allow better insulation of the series connection from the surrounding space, since the displacement current now flows all across the interface between the two nanocircuit elements, where the EVL connector is positioned. The electric field in the ENZ regions is parallel to this interface, but the low permittivity of these regions ensures that the displacement current leakage is very low. This behavior is confirmed in Fig. 6, where the displacement vec-

tor distribution **D**=ε**E** has been evaluated for the same geometry with a finite-element software.[20] Figure 6 confirms and validates our results using a different simulation technique, and it explains more evidently the improved agreement between circuit theory and simulations in this scenario around the resonance frequency (i.e., in the range of frequency in which the ENZ material has near-zero permittivity). It is evident how the displacement current flow is confined inside the two slabs, connected in series by an EVL material, due to the proper insulation ensured by ENZ lateral slabs. There is no electric displacement flow outside the nanofilter pair, and indeed near the resonance the pair of nanoelements may be interpreted as connected in series. Once again, the additional resonances observed in this nanofilter are due to the plasmonic resonance at the interfaces between regions with oppositely signed permittivities. Nevertheless, this nanocircuit exhibits stop-band behavior (albeit several bands), the main one of which is designed according to the analogous rf circuit theory. It is important to point out that dispersion characteristics of materials involved in such nanofilters may provide these filters with richer transfer functions that may be exploited in the overall response design.

In order to further underline the response and functionality of this stop-band series filter, Fig. 7 reports the behavior of the transfer function in this setup evaluated separately for the two nanocircuit elements, imagining to extract the signal at the two terminals of the nanoinductor (silver nanorod) and of the nanocapacitor (SiO₂ nanorod) separately. The plots compare the three cases of the geometry of Fig. 4 (black solid line), the geometry of Fig. 6 with nanoinsulators (green light line), and the ideal circuit response for the two elements.

There is good agreement between circuit theory and full-wave simulations, despite the abrupt change in the waveguide cross section and the dispersion of the materials. At the
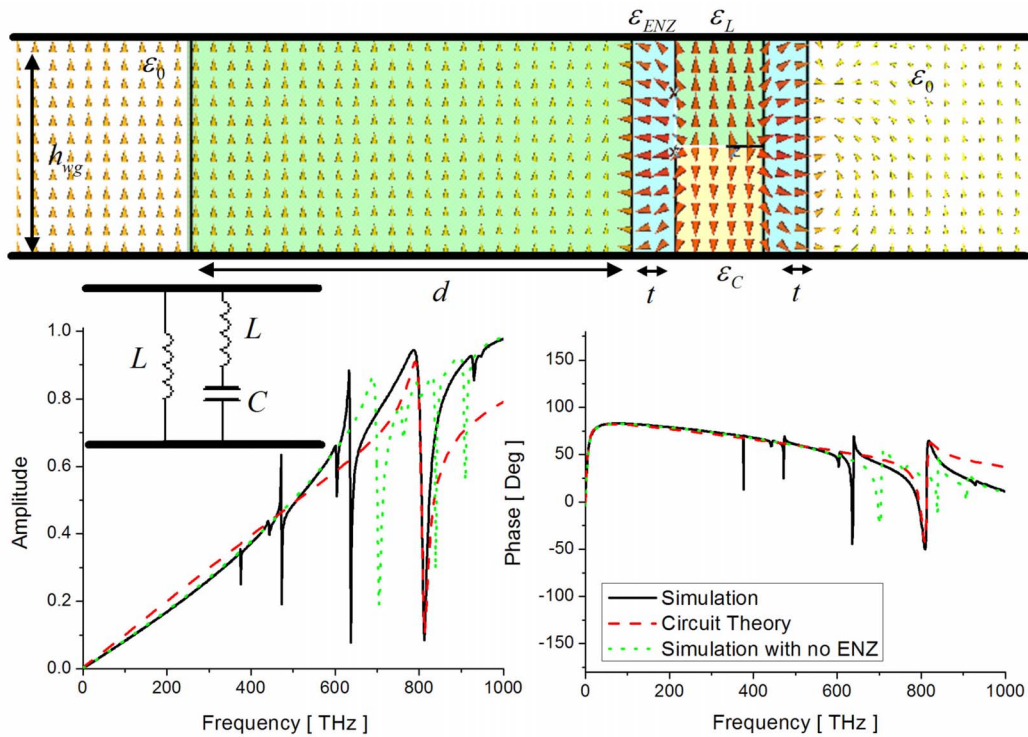
FIG. 11. (Color online) Electric field distribution at the resonant frequency of the series and transfer function for a third-order nanofilter made by cascading a series *LC* filter with a nanoinductor. The involved materials are assumed to be silver and silicon dioxide, plus ENZ material for the nanoinsulators. The black solid line refers to the simulation when ENZ nanoinsulators are used, the dashed red line refers to ideal circuit theory simulations, and the dotted green line refers to the same geometry, but without the use of ENZ nanoinsulators.

stop band, even though the signal is not transmitted through the nanofilter, the two elements by themselves experience a peak in their transfer function extracted across their terminals, with 180° shift between the *L* and *C*. This is consistent with the operation of a series *LC* stop-band filtering device.

E. Series combinations: Extraction of the individual element response

Up to now we have presented several examples on how basic nanofilters might be simply realized at optical frequencies following design rules analogous to those of their low-frequency counterparts. The last example provided us with an interesting difference between a high-frequency nanocircuit and a low-frequency circuit: despite the complex resonant response of the two individual nanoelements in Fig. 4 or 6, the response measured at the output terminal of the filter shows a general stop-band response—i.e., zero transmission at the resonance frequency (as well as at other resonant frequencies). In a classic circuit, however, it may be desirable to pick the voltage and current at one of the two individual elements (i.e., *L* or *C*), similar to what reported in Fig. 7. Not having ideal "terminals" at the end of each one of the nanocircuit elements, however, it appears more difficult in this scenario to actually extract such information from the individual elements in the series combination. However, following the concepts introduced in Refs. 7–10 and in the previous paragraphs, we can employ a nanoconnector to extract such signal from the center of the series connection.

Figure 8 shows the geometry that we analyze in this context: the EVL connector at the interface between the series elements of Fig. 6 has been extended down to the output terminal of the filter (here we have not employed ENZ insulators, since their presence is not crucial). In this scenario, as seen from the field distribution at the resonance, it is possible to "guide" the antiphase field distribution present inside the nanocircuit at the resonance (as predicted by Figs. 4–7) to the end of the waveguide, analogous with the optical "shorting wire" idea we have recently presented in Ref. 10. It is interesting to note that the electric field in the narrow EVL channel is indeed oriented longitudinally, consistent with the fact that the displacement current is being guided along the EVL "wire" to maintain the potential drop across the two elements in the empty region of the waveguide. This allows extraction of the signal from the individual elements in the series combination at the output of the filter, obtaining results that are consistent with those presented in Fig. 7. This might be a viable way to extract the transfer functions from individual optical nanocircuit elements in series.

F. Nanofilters at THz frequencies

We have also been interested in applying the concepts outlined in the previous paragraphs to nanocircuits at THz frequencies. At these frequencies, some semiconductors may exhibit anomalous values for real part of permittivities. For instance, SiC (Ref. 29), InSb (Ref. 30), and $LiTaO_3$ (Ref. 30) have relatively low absorption with windows of frequency
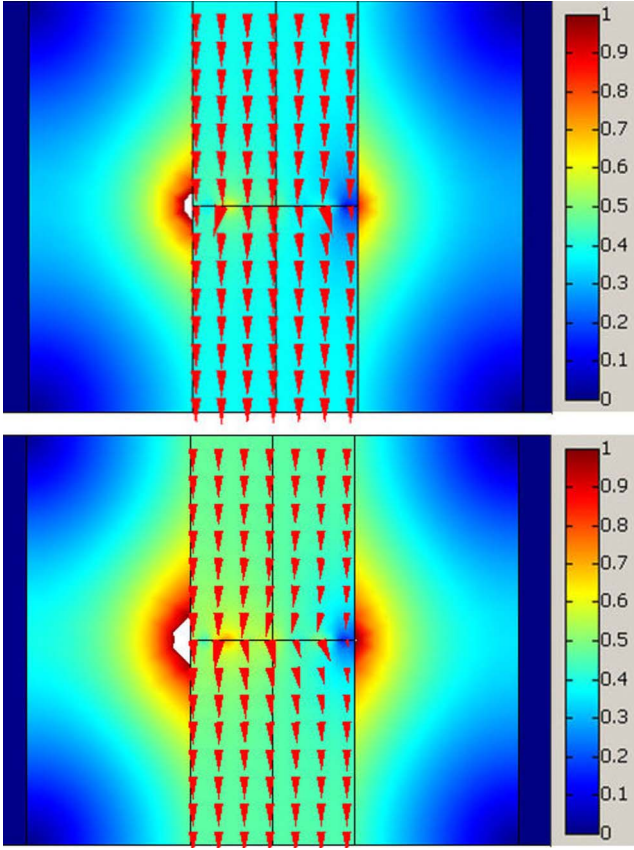
FIG. 12. (Color online) Electric displacement distribution for the geometry of Fig. 11 (top) and for the nanocapacitor connected in parallel with the *LC* structure (bottom), as evaluated using Ref. 20.

over which their relative permittivities may have negative, close to zero, or very high real part. This may provide another set of materials for use in our nanofilter concepts at infrared frequencies.

Even though the previous concepts are easily scalable to lower frequencies, the main difference is in the fact that the polaritonic frequency dispersion of such materials generally follows a Lorentzian model, and therefore the bandwidth over which these concepts are applied may become narrower than those in the previous examples. As we show below, such Lorentzian dispersion may actually provide additional degrees of freedom for the nanocircuit response. Moreover, a clear advantage of this range of frequency is that it may be less challenging to realize electrically smaller nanocircuit elements at these lower frequencies.

As an example, Fig. 9 reports the transfer function for a parallel resonant pair consisting of a SiC nanorod of dimensions $(d=250$ nm$)\times(h=100$ nm$)$ and permittivity ε_L satisfying a realistic Lorentzian model with losses for SiC (Ref. 29) in parallel with a dielectric nanorod of the same dimensions and with $\varepsilon_C=3\varepsilon_0$, embedded in a waveguide with $h_{wg}=h$. The results are consistent with the circuit theory and show how it is possible to obtain a good stop-band nanofilter in a parallel combination in this frequency regime. This is due to the fact that the zero in transmission coefficient is obtained at the material resonance of SiC, around 25 THz. The parallel resonance, arising in this design around 30 THz, brings back

the transfer function to unity and for this choice of parameters has a relatively wider bandwidth of operation (consistent with the previous discussion, since now $h_{wg}=h$).

Figure 10, as a further example, reports the case of a series combination obtained by combining a nanoinductor made of a Lorentzian material, with permittivity $\varepsilon_L=(1+6.7\frac{\omega_L^2-\omega_T^2}{\omega_T^2-\omega^2-i\omega\gamma})\varepsilon_0$ with $\omega_L=29.07$ THz, $\omega_T=23.79$ THz, and $\gamma=142.8$ GHz (the level of losses is analogous to those of SiC at THz frequencies), combined in series with a dielectric nanorod with $\varepsilon_C=10\varepsilon_0$. The two nanocircuit elements have both height $h=h_{wg}/2=250$ nm and length $d=2$ μm and they are separated by an EVL separator (20 nm thick) made of realistic LiTaO$_3$ material, with the Lorentzian model reported in Ref. 30. At the resonance frequency of 4.32 THz, $\varepsilon_{\text{LiTaO}_3}=(-373+i433)\varepsilon_0$, acting well as an EVL material in the range of frequency of interest. The electric field distribution at the resonance shows how LiTaO$_3$, despite its nonideal behavior with a high imaginary part, is capable of picking the resonant field distributions of two elements and guide them to the output of the waveguide, as described in the previous section. Moreover, the transfer function shows how the stop-band behavior coincides with the expected one from the circuit theory and the extracted voltages at the end of the waveguide confirm the presence of two resonant peaks for the signals extracted from L and C separately, with a zero transmission for the sum signal, consistent with the expected nanofilter response. In this geometry, it may therefore be possible to extract separately the signals applied to L and C at the end of the waveguide. The results are in good agreement with the frequency response of a resonant LC series filter.

III. DESIGN OF HIGHER-ORDER OPTICAL NANOFILTERS

After having presented the design of basic nanofilters at optical frequencies, in this section we show how even more complex configurations and frequency responses may be obtained by combining the previous concepts and having properly connected basic nanofilters forming more complex nanocircuits, similar to what is commonly done in regular low-frequency circuits.

Figure 11 refers to a third-order nanofilter, obtained by connecting in parallel a series LC filter with a nanoinductor. The two inductors are both made of silver, whereas the nanocapacitor consists of SiO$_2$. The dimensions of the parallel nanoinductor are assumed to be $(d=20$ nm$)\times(h=10$ nm$)$, whereas the two series nanorods have size $(d/5)\times(h/2)$. Moreover, the series elements are insulated by an ENZ material with thickness $t=4$ nm and a Drude model dispersion (1) with a plasma frequency selected to be around the resonant frequency of the series connection—i.e., $f_p=810$ THz, $\gamma=4$ THz.

The transfer function plots in Fig. 11 compare the circuit response for the circuit model depicted in the inset with the full-wave simulations obtained for the geometry of the figure and for the case in which the ENZ insulators are removed. The field distribution is shown at the resonant frequency of
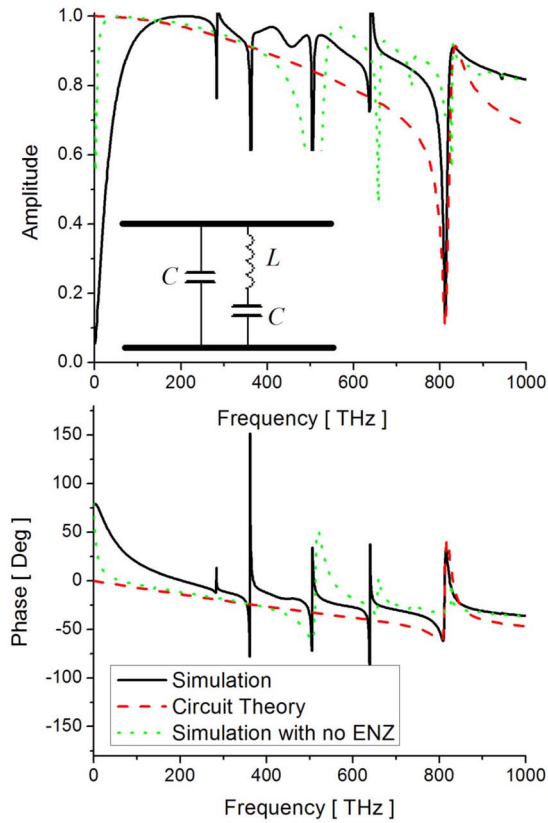
FIG. 13. (Color online) Transfer function for a nanofilter similar to Fig. 10, but substituting the parallel nanoinductor with a parallel nanocapacitor with $\varepsilon_C = 5\varepsilon_0$.

the series connection, where the zero of the filter response is expected (around f_p).

It is seen how the third-order filter combines the high-pass functionality of an *RL* filter with the stop-band feature of the *LC* series and therefore provides further degrees of freedom for the nanocircuit response. The extracted transfer function agrees qualitatively with the ideal one obtained from circuit theory (albeit with more resonances at lower frequencies due to plasmonic resonances at interfaces), and the presence of ENZ nanoinsulators to confine the displacement current in the series connection at its resonance leads to improving the agreement around f_p. The electric field distribution at the series resonance, shown in Fig. 11, confirms this prediction, highlighting the out-of-phase voltage drop in the two nanocircuit elements and the absence of current leakage outside of the pair, due to the nanoinsulators.

In Fig. 12, moreover, this behavior is confirmed and validated using Ref. 20, highlighting the displacement current flow at the series resonance of the nanofilter. It is noticeable how the displacement field is maximized and enhanced inside the series elements, similar to the response of a classic resonant filter, and no current leakage is allowed by the presence of the insulators.

Figure 13 corresponds to a different third-order filter, obtained by substituting the parallel nanoinductor of Fig. 12 with a parallel nanocapacitor with $\varepsilon_C = 5\varepsilon_0$. The sizes of the elements are the same, and the functionality of the nanofilter
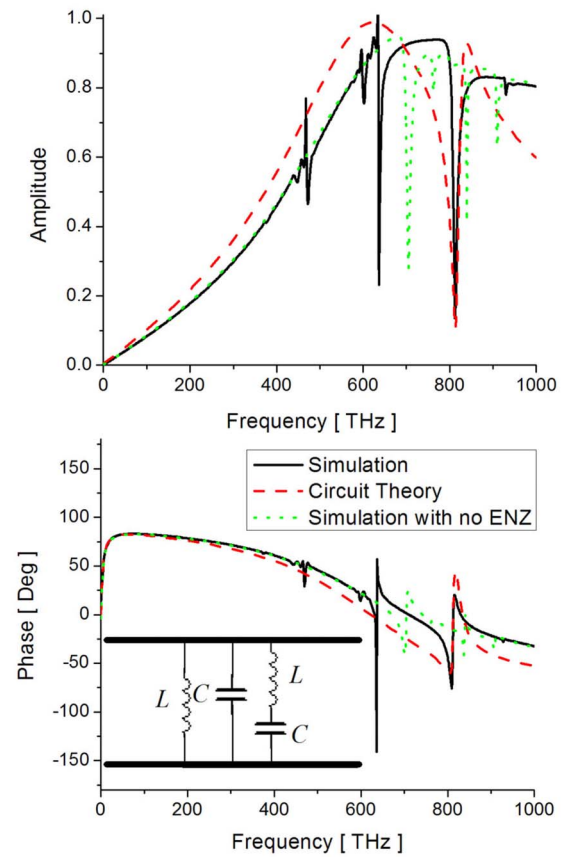

FIG. 14. (Color online) Electric displacement distribution (top) and transfer function (bottom) for a fourth-order nanofilter, obtained by combining in the geometry of Figs. 10 and 11 with both the parallel nanoinductor and nanocapacitor.

is now expected to combine the stop-band features of the series connection with the low-pass filtering of the parallel nanocapacitor. The simulations show this to be possible, and the comparison between the simulated results and the circuit response is fairly good qualitatively, considering the complexity of the nanocircuit. The presence of the insulators allows a fairly good agreement of the simulated and expected curves around the resonant frequency.

As a final example, we present in Fig. 14 the results for a fourth-order nanofilter, obtained by combining the geometries of Figs. 12 and 13 in order to have a series *LC* nanofilter in parallel with a parallel *LC*. In this case, the frequency response should give rise to two pass bands and a stop band, modulating a high-pass filter. This complex filter response is reasonably well obtained in the extracted response from the nanocircuit, both with and without the presence of the ENZ insulators. This final design shows how complex filtering response may be designed by utilizing plasmonic and non-plasmonic nanoparticles, suitably combined together and displaced in accordance with the impinging electric field.

IV. CONCLUSIONS

We have reported here our theoretical investigation on the possibility of employing plasmonic and nonplasmonic nano-

structures to design nanofilters and extend the functionalities of nanocircuits at infrared and optical frequencies. Relatively complex frequency responses have been obtained by employing plasmonic and dielectric nanoparticles to realize optical nanofilters with low-pass, high-pass, stop-band, and pass-band functionalities. The use of nanoinsulators and nanoconnectors has been proposed to reduce unwanted coupling among the different components of the nanofilters and to extract the frequency response from series nanocircuit elements. These results may be considered an informative step towards the realization of functional nanocircuits at THz and optical frequencies.

*Author to whom correspondence should be addressed: engheta@ee.upenn.edu

[1] R. Zhia, J. A. Schuller, A. Chandran, and M. Brongersma, Mater. Today **9**, (7-8), 20 (2006).

[2] N. Engheta, A. Salandrino, and A. Alù, Phys. Rev. Lett. **95**, 095504 (2005).

[3] N. Engheta, Science **317**, 1698 (2007).

[4] A. Alù and N. Engheta, J. Opt. Soc. Am. B **23**, 571 (2006).

[5] A. Alù and N. Engheta, Phys. Rev. B **74**, 205436 (2006).

[6] A. Alù and N. Engheta, Phys. Rev. B **75**, 024304 (2007).

[7] M. G. Silveirinha, A. Alù, J. Li, and N. Engheta, J. Appl. Phys. **103**, 064305 (2008).

[8] A. Alù, A. Salandrino, and N. Engheta, J. Opt. Soc. Am. B **24**, 3014 (2007).

[9] A. Alù, A. Salandrino, and N. Engheta, Opt. Express **15**, 13865 (2007).

[10] A. Alù and N. Engheta, Opt. Express **15**, 13773 (2007).

[11] R. W. Rendell and D. J. Scalapino, Phys. Rev. B **24**, 3276 (1981).

[12] X. C. Zeng, P. M. Hui, D. J. Bergman, and D. Stroud, Phys. Rev. B **39**, 13224 (1989).

[13] D. A. Genov, A. K. Sarychev, V. M. Shalaev, and A. Wei, Nano Lett. **4**, 153 (2004).

[14] S. Govindaswamy, J. East, F. Terry, E. Topsakal, J. L. Volakis, and G. I. Haddad, Microwave Opt. Technol. Lett. **41**, 266 (2004).

[15] A. I. Csurgay and W. Porod, Int. J. Circuit Theory Appl. **32**, 339 (2004).

[16] L. D. Landau and E. M. Lifshitz, *Electrodynamics of Continuous Media, Course of Theoretical Physics* (Elsevier Butterworth-Heinemann, Oxford, 2004), Vol. 8.

[17] C. F. Bohren and D. R. Huffman, *Absorption and Scattering of Light by Small Particles* (Wiley, New York, 1983).

[18] A. S. Sedra and K. C. Smith, *Microelectronic Circuits* (Oxford University Press, New York, 2003).

[19] www.cst.com

[20] www.comsol.com

[21] G. D. Mahan and G. Obermair, Phys. Rev. **183**, 834 (1969).

[22] A. Alù and N. Engheta, arXiv:0710.3411 (unpublished).

[23] A. Alù and N. Engheta, Nature Photonics, in press (2008).

[24] E. Shamonina, V. A. Kalinin, K. H. Ringhofer, and L. Solymar, Electron. Lett. **37**, 1243 (2001).

[25] S. A. Ramakrishna, J. B. Pendry, M. C. K. Wiltshire, and W. J. Stewart, J. Mod. Opt. **50**, 1419 (2003).

[26] S. Adachi, Phys. Rev. B **38**, 12966 (1988).

[27] P. B. Johnson and R. W. Christy, Phys. Rev. B **6**, 4370 (1972).

[28] I. H. Malitson, J. Opt. Soc. Am. **55**, 1205 (1965).

[29] W. G. Spitzer, D. Kleinman, and J. Walsh, Phys. Rev. **113**, 127 (1959).

[30] J. Gómez Rivas, C. Janke, P. Bolivar, and H. Kurz, Opt. Express **13**, 847 (2005).